Published in final edited form as:
Inorg Chem. 2011 March 21; 50(6): 2479–2487. doi:10.1021/ic102295s.

MAPping the Chiral Inversion and Structural Transformation of a Metal-Tripeptide Complex having Ni-SOD Activity

Mary E. Krause[1], **Amanda M. Glass**[1], **Timothy A. Jackson**[1,*], and **Jennifer S. Laurence**[2,*]

[1] Department of Chemistry, University of Kansas, Lawrence, KS 66045

[2] Department of Pharmaceutical Chemistry, University of Kansas, Lawrence, KS 66047

Abstract

The metal abstraction peptide (MAP) tag is a tripeptide sequence capable of abstracting a metal ion from a chelator and binding it with extremely high affinity at neutral pH. Initial studies on the nickel-bound form of the complex demonstrate that the tripeptide asparagine-cysteine-cysteine (NCC) binds metal with 2N:2S, square planar geometry and behaves as both a structural and functional mimic of Ni superoxide dismutase (Ni-SOD). Electronic absorption, circular dichroism (CD), and magnetic CD (MCD) data collected for Ni-NCC are consistent with a diamagnetic Ni^{II} center. It is apparent from the CD signal of Ni-NCC that the optical activity of the complex changes over time. Mass spectrometry data show that the mass of the complex is unchanged. Combined with the CD data, this suggests that chiral rearrangement of the complex occurs. Following incubation of the nickel-containing peptide in D_2O and back-exchange into H_2O, incorporation of deuterium into non-exchangeable positions is observed, indicating chiral inversion occurs at two of the alpha carbon atoms in the peptide. Control peptides were used to further characterize the chirality of the final nickel-peptide complex, and DFT calculations were performed to validate the hypothesized position of the chiral inversions. In total, these data indicate Ni-SOD activity is increased proportionally to the degree of structural change in the complex over time, as cross-correlation between the change in CD signal and change in SOD activity reveals a linear relationship.

Keywords

Chiral inversion; Ni-NCC; Metal Abstraction Peptide (MAP); D-amino acid; D-Cys; square planar; peptide-metal complex; Ni-SOD; superoxide dismutase

INTRODUCTION

The metal abstraction peptide (MAP) tag is a tripeptide, here with the sequence Asn-Cys-Cys (NCC).[1] A reaction with IMAC resin-chelated nickel allows this NCC peptide to react with and abstract the metal, resulting in a high affinity Ni-peptide complex at neutral pH. The nickel-bound peptide, Ni-NCC, contains a diamagnetic Ni^{II} center bound in square planar geometry (Figure 1) with 2N:2S coordination.[1] Computational analysis determined

[*]Authors to whom correspondence should be addressed: Jennifer S. Laurence: Telephone (785) 864-3405; Fax (785) 864-5736; laurencj@ku.edu, Timothy A. Jackson: Telephone (785) 864-3968; Fax (785) 864-5396; taj@ku.edu.

Supporting Information Available: Variable temperature MCD data for fresh and aged Ni-NCC, TD-DFT computations, *d* orbital energy level diagram for models of Ni-NCC, plots comparing changes in CD signal as a function of age at various pH, and Cartesian coordinates for models of Ni-NCC energy-minimized using DFT computations. This material is available free of charge via the internet at http://pubs.acs.org.

the structure of Ni-NCC has mixed amine/amide nitrogen coordination and *cis* deprotonated thiolates. This coordination is very similar to that of Ni in the enzyme nickel superoxide dismutase (Ni-SOD), which consists of two cysteinate sulfurs (Cys2 and Cys6) arranged *cis* to one another, the N-terminal amine, and the deprotonated amide nitrogen from the peptide backbone of Cys2.[2–4] When bound to nickel, the tripeptide acts a functional mimic of the enzyme nickel superoxide dismutase.[1] The reaction catalyzed by Ni-SOD is unusual as it employs oxidation-prone thiolate ligands to bind the redox-active Ni ion. Metal-centered redox cycling between the Ni^{II} and Ni^{III} states is necessary to afford Ni-SOD activity. Coordination of the metal ion in the protein shifts between square planar (Ni^{II}) and square pyramidal (Ni^{III}) and leaves one face of the Ni ion open to solvent or substrate binding and enzymatic turnover. Completmentary studies of the spectroscopic properties and reactivities of maquettes derived from a sequence of NiSOD have provided additional insights into the structure and mechanism of NiSOD.[5–9]

Our previous studies allowed the determination of ligands to the metal and the overall geometry of the Ni-NCC complex; however, a stability study has further revealed that the metal-tripeptide complex undergoes chiral inversion in a site-specific manner. This modification is distinctive, as chiral inversion is not often observed in proteins, and the structural change that occurs in this complex is both site and structurally specific. This chiral change has not been reported to occur in Ni-SOD or in small peptide maquettes derived from the N-terminal sequence, which contains the metal-binding loop. Amino acids and dipeptides are known to undergo base-catalyzed racemization at the chiral α-carbon as a result of metal chelation, but inversion is typically accomplished over several hours at highly elevated temperature (>90 °C) and basic pH (>9).[10–14] Studies performed on metal-amino acid chelates in deuterated solvent reveal that approximately an equal proportion of L and D isomers are generated during such reflux reactions in the absence of strong conformational influences. Because of the need for such extreme conditions, this type of reaction is not relevant to proteins expressed and purified using the typical range of conditions.

The D amino acids that have been observed in proteins and peptides often impart significant differences in biological function to the chiral peptide and protein variants; while some act as inhibitors, others act as activators.[15] The introduction of a D amino acid alters the structure of the peptide or protein,[16] which can in turn influence the biological activity of the parent peptide.[17,18] Conversely, chiral mutagenesis of proteins has been shown to stabilize certain proteins, including insulin.[19] All naturally occurring, biosynthetic peptides and proteins that contain D amino acids are first generated entirely from L amino acids, and the inversion occurs as a post-translational modification.

Three major methods of incorporation of D amino acids have been reported, and the majority of D amino acids are found within three amino acids of the N- or C-terminus. First, if the placement of the D amino acid is intentional, it is enzyme catalyzed by amino acid racemases.[15] While most of these racemases employ a pyridoxalphosphate cofactor and proceed through a Schiff-base intermediate, some are thought to follow a different mechanism that does not require this cofactor. Reported examples of known enzyme-catalyzed epimerization include an enzyme from the venom of the funnel web spider that catalyzes the conversion of Ser-46 to D-Ser 46 within a 48 residue peptide (ω-agatoxin IV),[15,18] an enzyme isolated from the skin of a frog (*Bombina*) that incorporates a D-amino acid into the second position of the substrate,[15,20] and a mammalian enzyme from platypus venom that has specific, but not completely known, substrate requirements.[21]

The only other reports of D amino acids in mammalian proteins are in aged tissues, and these aging proteins have been shown to contain D amino acids, largely at aspartic acid

residues, which are prone to racemization.[15,22] Examples of proteins and peptides containing D-Asp from this type of reaction include human lens alpha A-crystallin,[23] human lens alpha B-crystallin,[24] and beta-amyloid protein in the brain.[25] The presence of the D-Asp influences the behavior of the peptide and its effect on neurodegeneration in Alzheimer's patients.[26] These spontaneous inversions of chirality arise from a mechanism involving cyclization and hydrolysis reactions, where the nearby environment of the protein helps initiate and drive the conversion.[22]

The mechanisms described above are reversible reactions, but conversion of an amino acid from L to D chirality within proteins has also been reported to proceed via a free radical reaction, in which cysteine residues are involved in the electron transfer.[27] These reactions are light-driven and unidirectional. The cysteinyl radical is generated by intense UV light and subsequently abstracts hydrogen from a surrounding amino acid, leading to epimerization.[27–30] The selectivity determining where the reaction occurs is controlled by the secondary structure of the peptide or protein, leading to a variety of different products, depending on the context.[28]

Despite the limited number of examples of site-specific L to D conversions that have been reported, the literature reveals that diverse mechanisms are used to accomplish chiral inversion. To our knowledge, we report here the first site-specific chiral inversion of amino acids that depends on metal binding. The reaction proceeds at room temperature and near neutral pH in aqueous solution over the course of hours. While NCC was synthesized to contain all L amino acids, conversion to the D-containing form occurs after complexation with nickel, and the reaction results in inversion at two positions to produce the stable DLD-NCC-metal complex. The resulting DLD-peptide-metal complex is very stable in aqueous solution, and DFT calculations indicate that the change in chirality produces a large increase in thermodynamic stability.

EXPERIMENTAL

Generation of metal-peptide complexes

The peptides NCC, GCC, and NCC with a D-cysteine in the middle position [LDL-NCC] were purchased from Genscript Corporation (Piscatway, NJ, USA). The NCC peptides with a D-cysteine in the third position [LLD-NCC] and with both D-asparagine in the first position and D-cysteine in the third posistion [DLD-NCC] were purchased from Neo-Peptide (Cambridge, MA, USA). Nickel-peptide complexes were generated in aqueous solution at neutral to basic pH. Incubation of the peptide for approximately 30 minutes with immobilized metal affinity chromatography (IMAC) resin (GE Healthcare) charged with nickel ensures a clean reaction with no undesired side products and no free metal ions in solution, yielding a reddish-brown complex, varying slightly by the identity of the peptide. Aged Ni-NCC samples were allowed to age for >40 days.

CD and absorption studies

A 1.5 mM solution of Ni-NCC was prepared in 50 mM potassium phosphate, pH 7.4, and used as is or sparged with argon. Immediately after incubation, samples were placed in a cuvette with a 1-cm pathlength and scanned from 800-300 nm using both absorption and CD spectroscopy. Samples were aged and monitored at various timepoints over the course of several days. Background scans of buffer alone were subtracted from each scan. Absorption studies were performed on an Agilent 8453 UV/Visible spectrophotometer. Circular dichroism analysis was performed on a J-815 (Jasco Corporation) spectrapolorimeter. The CD data presented represent the average of at least five scans. To accurately control the time frame of Ni-NCC aging for activity assays, the complex also was formed in solution upon addition of one equivalent of $NiSO_4$.

MCD experiments

Samples of Ni-NCC were prepared in 50 mM potassium phosphate buffer at pH 7.4 sparged with argon. Solid sucrose was added as a glassing agent and the mixture was heated to form a saturated solution. CD spectra of sucrose-saturated samples demonstrated no significant changes in features compared with samples lacking sucrose, indicating that this procedure did not perturb the structures of the Ni-NCC complex. The samples were placed in an MCD cell and flash frozen in liquid N_2. Spectra were collected on a J-815 (Jasco Corporation) spectropolarimeter interfaced with a magnetocryostat (Oxford Spectromag 4000-8). To remove contributions from CD signals, MCD data reported herein represent difference spectra of accumulations at +7 and −7 T. Because the signal intensities from paramagnetic species display inverse temperature dependence, spectra were collected at several temperatures.

Deconvolution of CD and absorption data

Deconvolution of CD and absorption data was performed using Igor Pro (Wavemetrics). Iterative Gaussian deconvolutions were performed with a constant peak width of 1650 cm^{-1}. Absorption band energies were kept within 10% of the corresponding CD bands due to the broad nature of the absorption spectrum.

ESI-MS

Samples were diluted 100x in a 1:1 mixture of methanol/water and analyzed on an LCT Premier (Waters Corporation) operating in negative ion mode, as described previously.[1]

Deuterium exchange

A solution of 50 mM potassium phosphate was prepared in D_2O and adjusted with NaOD and DCl to a pD of 7.4. Samples of 1.5 mM NCC and GCC were prepared in this solution. Transmetallation was performed as described above. After removal of the solid resin, 10 μL of the sample was back-exchanged into one mL of a 1:1 water/methanol mixture and analyzed using ESI-MS operating in negative ion mode. The original samples were then incubated for 24 hours and analyzed in the same manner.

Electrochemistry

Electrochemical data were collected as previously described.[1] A 3 mL sample of 3 mM Ni-NCC was prepared in 50 mM sodium borate at pH 10. CV data were collected with a CH1812C Electrochemical Analyzer potentiostat (CH Instruments) with a three-electrode setup (platinum working electrode, Bioanalytical Systems, Inc.; Pt auxiliary electrode; Ag/AgCl reference electrode) in a glass CV cell. Potential was applied from zero to 1.2 V with a scan rate of 0.2 V per second, and current was measured. The same experiment was attempted on a 3 mM Ni-NCC sample in 50 mM potassium phosphate at the same pH. The sample was incubated for 24 hours and analyzed again.

Coordination of cyanide and IR analysis

Samples of Ni-NCC were prepared at a concentration of 3 mM in 50 mM sodium borate at pH 10 and 50 mM potassium phosphate at pH 7.4. A sample of Ni-NCC in phosphate buffer was incubated for 24 hours. One equivalent of potassium cyanide was added to each of the three Ni-NCC samples. Samples were flash frozen and lyophilized. IR analysis was performed to observe the cyanide peak in each sample. IR spectra were acquired from dry powder samples on a Perkin Elmer Spectrum 100 FT-IR spectrometer equiped with a universal ATR (Attenuated Total Reflection) sampling accessory. The spectrum of solid potassium cyanide was used to compare the shift of $\nu(C{\equiv}N)$ vibration from the free to the nickel-coordinated state.

Computations

Spin-restricted density functional theory (DFT) computations were performed using ORCA 2.8.0[31] and employed the conductor-like screening model (COSMO)[32] with an epsilon value of 80 to approximate water. Geometry optimizations used the BP86 functional[33,34] and the aug-TZVP basis set (a triple-zeta basis set with diffuse and polarization functions).[35,36] Because these computations employed the resolution of identity (RI) approximation,[37] the TZV/J auxiliary basis set was also used. Single point and time-dependent DFT (TD-DFT) computations used the B3LYP[38–40] functional and the aug-TZVP basis set. In order to evaluate if the inclusion of explicit water molecules H-bonded to charged groups gave rise to geometries markedly different than those obtained using COSMO, a water molecule was added to hydrogen bond with the C-terminal carboxylate in the LLL, DLD, and DDL models of Ni-NCC. Because differences in bond lengths of less than 0.015 Å were observed, we reasonably conclude that the use of COSMO is sufficient to account for major solvation effects in this system.

Ni-SOD xanthine/xanthine oxidase coupled assay

Ni-SOD activity was determined as reported previously,[1] except Ni-NCC was generated *in situ* using one equivalent $NiSO_4$. Ni-NCC was aged for 0 – 120 minutes, and the Ni-SOD activity was determined using the standard xanthine/xanthine oxidase method developed by Crappo and coworkers.[41] All reagents were generated in 50 mM potassium phosphate, 100 μM EDTA reaction buffer at pH 7.8 except for Ni-NCC, which was generated in 50 mM potassium phosphate, pH 7.4. 600 μM cytochrome c from bovine heart (Sigma), 300 μM xanthine (Sigma) and enough xanthine oxidase from buttermilk (Sigma) to cause a change in absorbance at 550 nM of 0.02 – 0.04 AU per minute were added to a final volume of 300 μL with reaction buffer. The change in absorbance at 550 nm was monitored on a Cary 100 UV-Visible spectrophotometer (Varian). The assay was performed with 100 μM Ni-NCC.

RESULTS

Preparation and spectroscopic characterization of Ni-NCC

As previously reported, metal incorporation into the described complex is most efficiently accomplished via transmetallation.[1] Peptides were incubated with IMAC resin in either 50 mM potassium phosphate buffer at pH 7.4 or in 50 mM sodium borate at pH 10. Absorption and CD spectroscopies were utilized to characterize the Ni-NCC complex. Studies have shown that pH, ionic strength, and concentration of the metal-peptide complex do not change the spectral features of the system;[1] however, these studies show that the initial spectra differ between buffer systems (Figure 2) but later converge to a common final state. pH is not a factor in the differences between spectra, as Ni-NCC samples analyzed in phosphate buffer at pH 10 directly after incubation exhibit the same spectral features as those in phosphate buffer at pH 7.4.

Over time, however, the spectral features of Ni-NCC in phosphate buffer change to resemble those in borate buffer, suggesting rearrangement to a more stable structure occurs. Although samples were prepared in sparged solutions, no further precautions were taken to avoid oxygen dissolution during aging. To ensure complete conversion, a Ni-NCC sample in phosphate buffer was aged in air for up to 90 days and analyzed again (Figure 3). ESI-MS of the Ni-NCC complex in various conditions demonstrated that the peptide mass does not change with the changes in spectral features (m/z = 392.98), indicating a lack of oxidation of thiolate ligands. Varied pH did not affect the overall rate of the aging process (Supporting Information; Figure S5). This suggests that the changes observed in the CD are due to more subtle changes about the metal center. A Ni-GCC sample was examined in the same manner to evaluate the influence of the chirality at the first position. Although the spectral changes

for the two complexes are not identical, a similar perturbation of CD signals was observed for Ni-GCC over a comparable time frame (data not shown).

Spectral deconvolutions

In contrast to the changes in the CD spectra of Ni-NCC, absorption spectra of Ni-NCC freshly prepared in phosphate buffer and that same sample aged for 40 days appear nearly identical (Figure 4a). Both feature a broad envelope centered at 21 000 cm^{-1} (ε = 210 $M^{-1}cm^{-1}$) with a higher energy feature at 29 000 cm^{-1} (ε = 1400 $M^{-1}cm^{-1}$). These data are consistent with both species having a four-coordinate Ni^{II} center in an N_2S_2 square planar geometry.[1] To quantitatively evaluate the CD spectral changes, spectral deconvolutions of these data were performed to determine the energies and signs of the electronic transitions (Figure 4b). Whereas freshly prepared Ni-NCC displays signals with positive sign at 18 900, 22 170, and 26 520 cm^{-1}, the spectrum of the aged sample shows negative bands at similar energies (Table 1). These transitions shift to slightly lower energies (Δ~200 – 900 cm^{-1}) with age. Bands 1 – 4 of freshly prepared Ni-NCC were previously assigned as *d-d* transitions[1] and their energies should be very sensitive to changes in geometry about the Ni^{II} center. The observation that the energies of these bands shift by < 900 cm^{-1} upon aging demonstrates that fresh and aged Ni-NCC have nearly identical coordination environments. The major spectral perturbations are predominately due to changes in sign and intensity of CD features. These minor changes in the *d-d* transition energies (Table 1) along with the virtually identical absorption spectra (Figure 4a) of fresh and aged Ni-NCC demonstrate that the geometry and ligands of the Ni^{II} center are unaltered and that neither dimerization of the complex nor oxidation of the thiolate ligand occurs.

Magnetic circular dichroism

To investigate whether a paramagnetic, tetrahedral intermediate is formed, magnetic CD (MCD) experiments were perfomed. Previous MCD expriments have shown that the primary Ni-NCC species in borate buffer at pH 10 is largely diamagnetic, although a minor paramagnetic (S=1) species was present.[1] Here, MCD experiments performed on a freshly prepared Ni-NCC sample demonstrated that the species initially present in phosphate buffer is also primarily diamagnetic; a minor paramagnetic component that accounts for less than 1% of the sample may reflect an intermediate state that does not accumulate. (Supporting Information: Figure S1) After aging, these temperature-dependent signals are no longer observed. Therefore, it can be concluded that aged Ni-NCC contains neither appreciable amounts of S = 1 Ni^{II} or S = 1/2 Ni^{III} centers. These data collectively show that both fresh and aged Ni-NCC contain diamagnetic Ni^{II} centers in square planar geometries with nearly identical coordination spheres; the differences in spectral features and in reactivity between the freshly prepared and aged samples led to further investigation of the subtle changes in the Ni-NCC complex.

Electrochemistry and reactivity of Ni-NCC

Previous electrochemical experiments have shown that Ni-NCC in borate buffer at pH 9.3 has a midpoint potential of 0.72 V (vs. Ag/Ag^+).[1] When attempts to measure the midpoint potential of Ni-NCC in phosphate buffer at the same pH were made, the complex prepared in phosphate buffer did not exhibit a measurable potential; however, when the same sample was aged for 24 hours, the midpoint potential was comparable to that of the sample in borate buffer (0.71 V vs. Ag/Ag^+). Previous studies have shown that square planar geometries, for example peptide mimics of Ni-SOD, coordinate cyanide in an axial position, as determined by IR of the bound cyanide.[42] Similarly, IR experiments have demonstrated that Ni-NCC in borate buffer is capable of coordinating CN^- in the axial position, as a shift in the $\nu(C\equiv N)$ vibration occurs. The IR spectrum of Ni-NCC freshly prepared in phosphate buffer did not exhibit a peak corresponding to coordinated cyanide; however, addition of cyanide after

aging the sample overnight generated the expected peak for the coordinated state (Table 2). These data lend support to a slow structural rearrangment that occurs over the course of hours, resulting in a structure that allows for the interaction of a fifth ligand with the Ni-NCC complex.

Deuterium exchange

The flip in sign of CD signals suggests the structural change that allows for ligand binding may be due to chiral inversion. Because of this possibility, NCC was transmetallated with Ni-IMAC resin in buffers prepared in D_2O to determine if deuterium would be incorporated into the peptide at any non-exchangeable site. After back-exchanging the Ni-NCC into 1:1 water/methanol to preserve the integrity of the complex but remove any exchangeable deuterium atoms, ESI-MS demonstrated incorporation of deuterium into two non-exchangeable positions (392.98 vs. 394.99). ESI-MS of the same reaction performed in H_2O showed no difference in m/z over 24 hours. Because Ni-GCC shows a similar inversion of CD signals with time, but lacks chirality in the first position, Ni-GCC was also examined for deuterium exchange. Ni-GCC exhibited incorporation of deuterium into one non-exchangeable position, suggesting that the chirality of Asn in the first position and only one of the Cys is affected. This information was used to predict the possible location(s) of the incorporated deuterium atom(s).

Characterization of peptides containing D amino acids

The LDL-Ni-NCC, LLD-Ni-NCC, and DLD-Ni-NCC complexes were generated and each analyzed using absorption and CD spectroscopies and ESI-MS. All of the complexes exhibit the same mass profile (m/z=392.98) in ESI-MS, suggesting that each forms 1:1 complexes with the metal. To determine the chirality of the final, stable Ni-NCC arrangement, CD spectra of each D-containing peptide were compared to the data collected for the aged (>40 days) Ni-NCC sample in phosphate buffer. The DLD-Ni-NCC spectrum overlaid with the aged Ni-NCC spectrum shows parallel features (Figure 5). These data indicate chiral inversion occurs at the first and third position within Ni-NCC to generate the DLD-Ni-NCC complex.

Whereas the spectral features of DLD-Ni-NCC do not shift or lose intensity with time, the CD spectrum of LLD-Ni-NCC evolves over time to look like that of DLD-Ni-NCC (Figure 6). In contrast, the CD spectrum of aged LDL-Ni-NCC looks like the mirror image of that of DLD-Ni-NCC. When the freshly prepared peptides were reacted with cyanide, only DLD-Ni-NCC was able to immediately coordinate cyanide in the axial position, providing further evidence that the DLD-form is the arrangment that aged Ni-NCC reaches over time.

DFT-Optimized Models and Computed Energies

Computations were performed on models of Ni-NCC to explore the structural and energetic changes associated with chiral inversion of the different amino acid residues in the tripeptide-Ni^{II} complex. These results are summarized in Table 3. In the optimized structure of LLL-Ni-NCC, the nickel(II) ion is bound in a near-square planar geometry (Figure 7). The coordination of the terminal amine, internal amide, and sulfur of Cys2 form two five-membered chelate rings that share a common edge. The sulfur of Cys3 coordinates *trans* to the amide nitrogen, which requires that the peptide wrap around the nickel center, thereby blocking one coordination site perpendicular to the square plane. The other open coordination site is partially blocked by the Asn side chain. These results suggest that the metal center may be sterically occluded in the LLL-peptide complex, explaining the lack of CN^- coordination observed in the freshly prepared samples described above.

The energies of Ni-NCC models with the chirality of different amino acids inverted show that inversion of Asn1 leads to a model (DLL-Ni-NCC) that is isoenergetic to that of LLL-Ni-NCC. In addition, the models in which Cys2 is inverted, LDL- and DDL-Ni-NCC, have an energetic destabilization of ~5 kcal/mol when compared to LLL-Ni-NCC. In contrast, when Cys3 is inverted, as in LLD- and DLD-Ni-NCC, an energetic stabilization of ~11 kcal/mol is predicted. Investigation into the role of solvation on the total energy of the conformers shows that although DLD-Ni-NCC does have an overall stabilization with respect to LLL-Ni-NCC in solvation energy, the relief of steric strain of the loop containing Cys3 has a more pronounced effect on the total energy. These results for DLD-Ni-NCC agree with the experimental data described above (Figure 5). The inversion from LLL-Ni-NCC to DLD-Ni-NCC opens one face of the Ni^{II} ion to interact with exogenous ligands, consistent with the observation that aged Ni-NCC binds CN^{-}.

TD-DFT computations

TD-DFT computations were performed to determine if the structural differences between LLL-Ni-NCC and DLD-Ni-NCC can account for the experimentally observed red-shift in the Ni^{II} *d-d* transition energies upon aging of Ni-NCC. Because Ni-S bond lengths are frequently overestimated in DFT geometry-optimized models, it is expected that the predicted electronic transition energies for both Ni-NCC models will be computed at lower energy than experimentally observed. Nonetheless, this known shortcoming in DFT-computed Ni-S bond lengths[43] will not hinder the analysis performed here, as the focus is on reproducing the relative shift in Ni^{II} *d-d* transitions between LLL-Ni-NCC and DLD-Ni-NCC. For an $S = 0$, d^8 metal ion in a square planar geometry, four *d-d* transitions are expected from excitation from each of the four doubly-occupied d orbitals to the unoccupied $d_{x^2-y^2}$ orbital. The computed energies of these transitions are shown in Table 4; corresponding spectra are shown in Supporting Information (Figure S2). Relative to LLL-Ni-NCC, all calculated *d-d* transitions for DLD-Ni-NCC are red-shifted, consistent with the experimental observation. This shift in transition energies is directly related to the energy of the $d_{x^2-y^2}$ orbital. In an idealized square planar geometry (*e.g.*, D_{4h} symmetry), the $d_{x^2-y^2}$ orbital is the dominant σ* orbital and is significantly destabilized relative to the remaining four d orbitals. As the geometry is perturbed from this limit, other d orbitals take on partial σ* character. This leads to the $d_{x^2-y^2}$ orbital being at a relatively lower energy and a red shift in *d-d* transitions. The nickel(II) coordination sphere in DLD-Ni-NCC is more distorted from square planar geometry than that of LLL-Ni-NCC, which gives rise to a smaller splitting between the Ni^{II} d orbitals (Supporting Information: Figure S3) and thus red shifted *d-d* transitions.

TD-DFT computations performed for DDL-Ni-NCC predict the three lower-energy *d-d* transitions to shift to higher-energy relative to LLL-Ni-NCC, which is inconsistent with experimental data. Taken together, both the total energies of the Ni-NCC models and the results of these TD-DFT computations are consistent with aged Ni-NCC corresponding to DLD-Ni-NCC, where the chirality of Asn1 and Cys3 have been inverted.

Ni-SOD Activity

The Ni-SOD activity assay was performed in order to probe whether the structural rearrangement that Ni-NCC undergoes while aging has an affect on the ability of the complex to consume the toxic anion superoxide. We previously showed that Ni-NCC behaves as a functional mimic of Ni-SOD, with an IC50 value of 41 μM.[1]

As computational analysis revealed, the final low-energy conformation, DLD-Ni-NCC, results in a more exposed Ni ion for solvent accessibility and reactivity with exogenous ligands. This is supported experimentally by the observed increase in SOD activity over

time, as well as the lack of cyanide binding to Ni-NCC initially, prior to chiral inversion.[1] Control experiments with $NiSO_4$ verify SOD activity is only detected when Ni-NCC is present in solution. SOD activity was measured at several time points while the Ni-NCC complex was aged. The activity change, as determined using the xanthine/xanthine oxidase assay, increased linearly with respect to time over the first several hours of the experiment. The initial activity was subtracted from the value measured for each aged sample, and these data were fit to a linear equation. Two replicants involving a total of 12 data points were analyzed to compare the change in SOD activity with the change in chirality of the aged Ni-NCC complex between 0 and 90 minutes. The data comparison shows a linear correlation between these two parameters with R2 values of 0.9242 and 0.9543 (data not shown). In addition, the functional data were compared to the intensity changes in the CD spectra at the same time points during the aging process. A linear relationship between SOD activity and chiral inversion was observed ($R^2 = 0.9592$), revealing a direct correlation between this structural change and SOD activity of the Ni-NCC complex (Figure 8).

Finally, after examining the control DLD complex immediately following formation, the IC50 value was determined to be 39 μM, which is the same as the aged LLL-Ni-NCC species, indicating conversion to the DLD isoform confers activity.

DISCUSSION

Structural rearrangment of Ni-NCC

Metal incorporation into the described Ni-NCC complex is accomplished rapidly (within seconds) via transmetallation[1]. The studies described here show that, following complex formation, chiral inversion occurs over the course of hours to generate the DLD isoform, which correlates to SOD activity. The initial CD spectra acquired immediately following metal abstraction by the peptide differ among buffer systems but later converge to a common final state. Neither varied pH (7–10) nor oxygen concentration affects the overall rate of the aging process, but the spectral differences observed between buffer systems are dramatic. Samples prepared in borate buffer reach the rearranged, final state much faster than samples prepared in phosphate buffer. The Ni-NCC samples prepared in borate buffer also immediately coordinate cyanide in the axial position, while the Ni-NCC samples prepared in phosphate buffer must be aged overnight before cyanide coordination can be detected. As mentioned above, these data lend support to a slower structural rearrangement that occurs over the course of hours-days, resulting in a structural state that allows for the interaction of a fifth ligand with the Ni-NCC complex. Similarly, Ni-NCC prepared in borate buffer has a midpoint potential that can be measured immediately using CV, whereas samples prepared in phosphate buffer must be aged overnight before any electrochemical signal is observed. These studies demonstrate that there is a difference between the final and initial arrangements of Ni-NCC that are observed in different buffer systems. The initial state is likely the all L-coordinated square planar arrangement, which the DFT computations suggest would be sterically hindered from binding even small ligands, *i.e.* CN^- and superoxide. Furthermore, MCD experiments reveal that both the Ni-NCC species measured immediately after complexation and then after aging are predominantly S=0 square planar.

The differences in spectral features and in reactivity between the freshly prepared and aged samples of Ni-NCC prompted further investigation of the subtle changes in the Ni-NCC complex. Using spectroscopic and ESI-MS studies, including those involving deuterium exchange, it was proposed that a change in the chirality of specific residues within this metal-peptide complex occurs as a result of metal binding. The incorporation of deuterium into non-exchangeable positions further supports chiral rearrangement.

Studies on the control peptides, GCC and those containing D-amino acids in various positions, helped elucidate the positions directly influenced by chiral inversion. A Ni-GCC sample was examined in the same manner to evaluate the influence of chirality at the first alpha carbon position. Although the spectra for these two complexes are not expected to be identical, a similar trend was observed for Ni-GCC in a similar time frame, suggesting that conversion occurs in the second and/or third positions. Recalling that NCC increased in mass by 2 amu during the deuterium exchange experiment, but GCC only increased by 1 amu and additionally taking into consideration that Gly is achiral, the data collectively indicate that only one of the Cys residues undergoes chiral inversion and that in NCC the first residue is also altered.

To determine which cysteine residue undergoes chiral inversion, the D-containing peptide complexes LDL-Ni-NCC, LLD-Ni-NCC, and DLD-Ni-NCC were characterized. All of the complexes exhibit the expected mass profile when examined using ESI-MS, suggesting that the same moieties from each of these peptides participate to accomplish metal binding using the same geometry. In general, inversion of the chirality at the metal center leads to CD spectra that are complete mirror images of one another;[44] however, changes in the CD spectra cannot be easily assigned to chiral inversions at individual positions in the peptide, and as such, the best indicator of the chirality of the final stable state is obtained through comparison to standards.

By overlaying the spectra of the D-containing peptides with the aged Ni-NCC spectra, it is evident that the DLD-Ni-NCC spectrum displays the same features as the aged Ni-NCC spectrum. These data further indicate chiral inversion occurs at the first and third position within Ni-NCC to generate the DLD-Ni-NCC complex. Moreover, it is obvious that the data for the aged all-L peptide does not correspond to inversion in the central position (Cys2), as the LDL peptide yields a spectral mirror image of the aged complex. The changes observed in the aged LLL complex rather closely, but do not exactly, parallel those associated with D-Cys in the third position, as demonstrated by comparison to LLD-Ni-NCC. All of the possible permutations of chirality were tested with DFT, showing the DLD form to be the most thermodynamically favorable. Based on the DFT calculations, there is a very large difference in energy between the peptides containing an L or D amino acid in that third position, strongly corroborating that the DLD peptide-metal complex is highly favorable.

The Ni-NCC complex was previously shown to mimic the Ni-SOD reaction in which a single electron is transferred through the metal center.[1] Here we show that the SOD activity of Ni-NCC increases as the complex ages, and the activity is linearly and directly related to the structural rearrangement of the complex. Although the structural rearrangement was unknown at the time of our previous report[1], the IC50 (data not shown) of the aged Ni-NCC sample is comparable with that value, indicating the original IC50 reflected a mostly chirally converted Ni-NCC species. The direct measurement of the DLD complex also has a comparable IC50, indicating this is the species with SOD activity. Chiral inversion has not been observed in the Ni-SOD protein or small peptide maquettes that have been used to probe the mechanism and structure of this protein. Although metal binding is accomplished with the same geometry and direct coordinating atoms in both cases, the connectivity among these atoms is not analogous. As the data and computations indicate, structural rearrangement of Ni-NCC from LLL to DLD promotes SOD activity by overcoming the steric hinderance that blocks ligand access to the axial position. Chiral inversion results in a substantially more favorable energy for the complex and a structure in which one face of the square planar Ni^{II} ion becomes more available for interaction with solvent, exogenous ligand, or potential substrate.

CONCLUSION

Here we have described the first metal-catalyzed site-specific chiral inversion of amino acids within a peptide. While a previous study defined the ligands involved in metal coordination and the geometry by which the metal is bound,[1] this study has elaborated the organization of the peptide in the complex and specifically shown that chiral inversion occurs at the first and third Cα positions in the NCC sequence. An intramolecular hydrogen transfer occurs through an intermediary carbon-centered radical to generate the more thermodynamically stable DLD-Ni-NCC configuration. This stable isomer appears to be responsible for the majority of the SOD activity of Ni-NCC.

Supplementary Material

Refer to Web version on PubMed Central for supplementary material.

Acknowledgments

We thank Drs. C. Schöneich and O. Mozziconacci for input on cysteinyl radicals and insight into chiral peptide studies, Dr. K. Frankowski for assistance with IR, and Drs. S. Lunte, M. Hulvey, and C. Kuhnline for assistance with CV. This work was supported by the J. R. and Inez Jay Fund (Higuchi Biosciences Center). M.E.K. is funded by the Madison and Lila Self Graduate Fellowship. A.M.G. is funded by the NIH Dynamic Aspects of Chemical Biology Training Grant (T2 GM GM08454) and the NSF GK-12 Fellowship (0742523).

References

1. Krause ME, Glass AM, Jackson TA, Laurence JS. Inorg Chem. 2010; 49:362–364. [PubMed: 20000358]
2. Szilagyi RK, Bryngelson PA, Maroney MJ, Hedman B, Hodgson KO, Solomon EI. J Am Chem Soc. 2004; 126:3018–3019. [PubMed: 15012109]
3. Wuerges J, Lee JW, Yim YI, Yim HS, Kang SO, Carugo KD. Proc Natl Acad Sci USA. 2004; 101:8569–8574. [PubMed: 15173586]
4. Barondeau DP, Kassmann CJ, Bruns CK, Tainer JA, Getzoff ED. Biochemistry. 2004; 43:8038–8047. [PubMed: 15209499]
5. Fiedler AT, Brunold TC. Inorg Chem. 2007; 46:8511–8523. [PubMed: 17305331]
6. Fiedler AT, Bryngelson PA, Maroney MJ, Brunold TC. J Am Chem Soc. 2005; 127:5449–5462. [PubMed: 15826182]
7. Shearer J, Dehestani A, Abanda F. Inorg Chem. 2008; 47:2649–2660. [PubMed: 18330983]
8. Shearer J, Long LM. Inorg Chem. 2006; 45:2358–2360. [PubMed: 16529443]
9. Neupane KP, Shearer J. Inorg Chem. 2006; 45:10552–10566. [PubMed: 17173410]
10. Buckingham DA, Marzilli LG, Sargeson AM. J Am Chem Soc. 1967; 89:5133–5138. [PubMed: 6065042]
11. Keyes WE, Caputo RE, Willett RD, Legg JI. J Am Chem Soc. 1976; 98:6939–6945. [PubMed: 965657]
12. Smith GG, Khatib A, Reddy GS. J Am Chem Soc. 1983; 105:295–297.
13. Stadtherr LG, Angelici RJ. Inorg Chem. 1975; 14:925–930.
14. Pasini A, Casella L. J Inorg nucl Chem. 1974; 36:2133–2144.
15. Jilek A, Kreil G. Monatshefte fur Chemie. 2008; 139:1–5.
16. Bobde V, Beri S, Rawale S, Satyanarayana CVV, Durani S. Tetrahedron. 1995; 51:3077–3086.
17. Kreil G. Annu Rev Biochem. 1997; 66:337–345. [PubMed: 9242910]
18. Heck S, et al. Science. 1994; 266:1065–1068. [PubMed: 7973665]
19. Nakagawa SH, Hua Q-x, Hu S-Q, Jia W, Wang S, Katsoyannis PG, Weiss MA. J Biol Chem. 2006; 281:22386–22396. [PubMed: 16751187]

20. Jilek A, Molay C, Tippelt C, Grassi J, Mignogna G, Mþllegger J, sander C, Fehrer C, Barra D, Kreil G. Proc Natl Acad Sci. 2005; 102:4235. [PubMed: 15758070]
21. Bansal PS, Torres AM, Crossett B, Wong KKY, Koh JMS, Geraghty DP, Vandenberg JI, Kuchel PW. J Biol Chem. 2008; 283:8969–8975. [PubMed: 18158286]
22. Fujii N. Biol Pharm Bull. 2005; 28:1585–1589. [PubMed: 16141520]
23. Fujii N, Satoh K, Harada K, Ishibashi Y. J Biochem (Tokyo). 1994; 116:663–669. [PubMed: 7852288]
24. Fujii N, Ishibashi Y, Satoh K, Fujino M, Harada K. Biochim Biophys Acta. 1994; 1204:157–163. [PubMed: 8142454]
25. Roher AE, Lowenson JD, Clarke S, Wolkow C, Want R, Cotter RJ, Reardon IM, Zurcher-Neely HA, Heinrikson R, Ball MJ, Greenberg BD. J Biol Chem. 1993; 268:3072–3083. [PubMed: 8428986]
26. Kubo T, Nishimura S, Kumagae Y, Kaneko I. J Neurosci Res. 2002; 70:474–483. [PubMed: 12391608]
27. Nauser T, Schöneich C. J Am Chem Soc. 2003; 125:2042–2043. [PubMed: 12590520]
28. Mozziconacci O, Williams TD, Kerwin BA, Schöneich C. J Phys Chem B. 2008; 112:15921–15932. [PubMed: 19368019]
29. Schöneich C. Chem Res Toxicol. 2008; 21:1175–1179. [PubMed: 18361510]
30. Mozziconacci O, Sharov V, Williams TD, Kerwin BA, Schöneich C. J Phys Chem B. 2008; 112:9250–9257. [PubMed: 18611046]
31. Neese, F. Version 2.8 ed. University of Bonn; 2009.
32. Sinnecker SR, Klamt A, Diedenhofen M, Neese F. J Phys Chem A. 2006; 110:2235–2245. [PubMed: 16466261]
33. Becke AD. J Chem Phys. 1986; 84:4524–4529.
34. Perdew JP. Phys Rev B. 1986; 33:8822–8824.
35. Schaefer A, Horn H, Ahlrichs R. J Chem Phys. 1992; 97:2571–2577.
36. Schaefer A, Huber C, Ahlrichs R. J Chem Phys. 1994; 100:5829–5835.
37. Neese F. J Comput Chem. 2003; 2003:1740–1747. [PubMed: 12964192]
38. Becke AD. J Chem Phys. 1993; 98:1372–1377.
39. Becke AD. J Chem Phys. 1993; 98:5648–5652.
40. Lee C, Yang W, Parr RG. Phys Rev B. 1988; 37:785–789.
41. Crapo JD, McCord JM, Fridovich I. Methods Enzymol. 1978; 53:382–393. [PubMed: 362127]
42. Tietze D, Breitzke H, Imhof D, Koeth E, Weston J, Buntkowsky G. Chem--Eur J. 2009; 15:517–523.
43. Bruschi M, De Gioia L, Zampella G, Reiher M, Fantucci P, Stein M. J Biol Inorg Chem. 2004; 9:873–884. [PubMed: 15365900]
44. Amouri, H.; Gruselle, M. Chirality in Transition Metal Chemistry: Molecules, Supramolecular Assemblies, and Materials. Wiley; 2009. Chirality and Entantiomers.

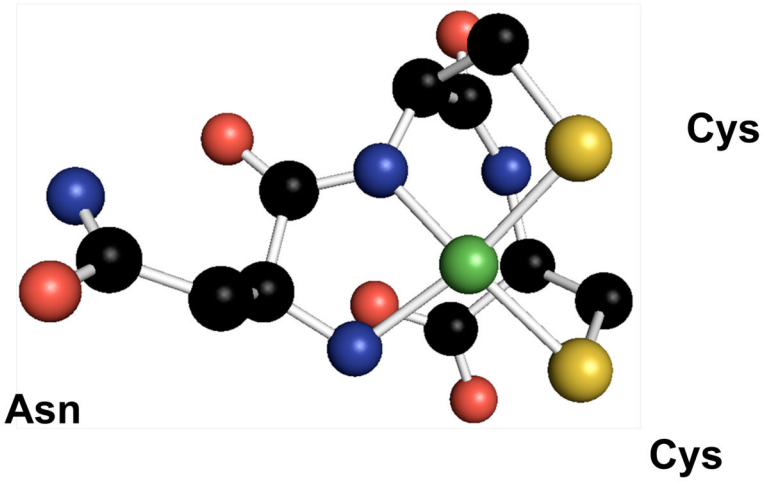

Figure 1.
Chemical structure of Ni-NCC showing the square planar arrangement of 2N:2S coordination around the nickel ion.

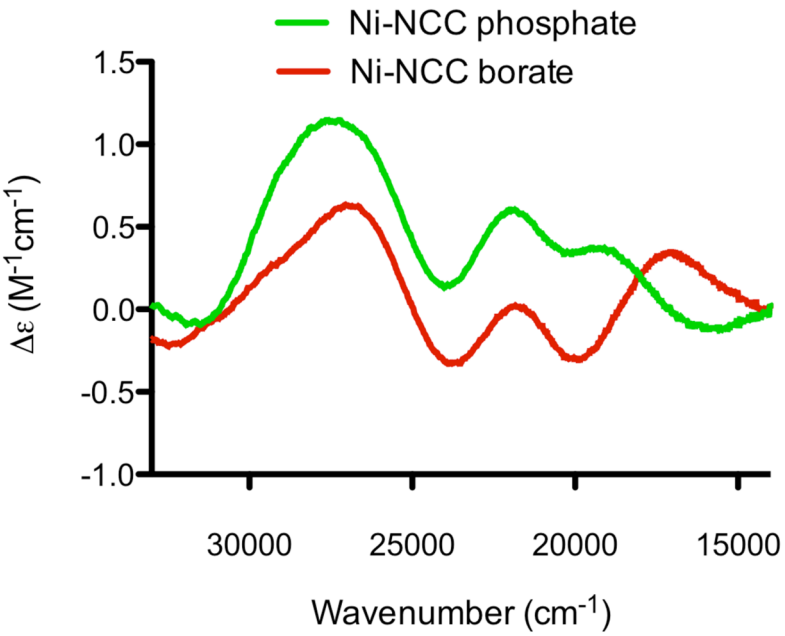

Figure 2.
In different buffer systems, Ni-NCC has different CD spectral features. (Green=phosphate, Red = borate).

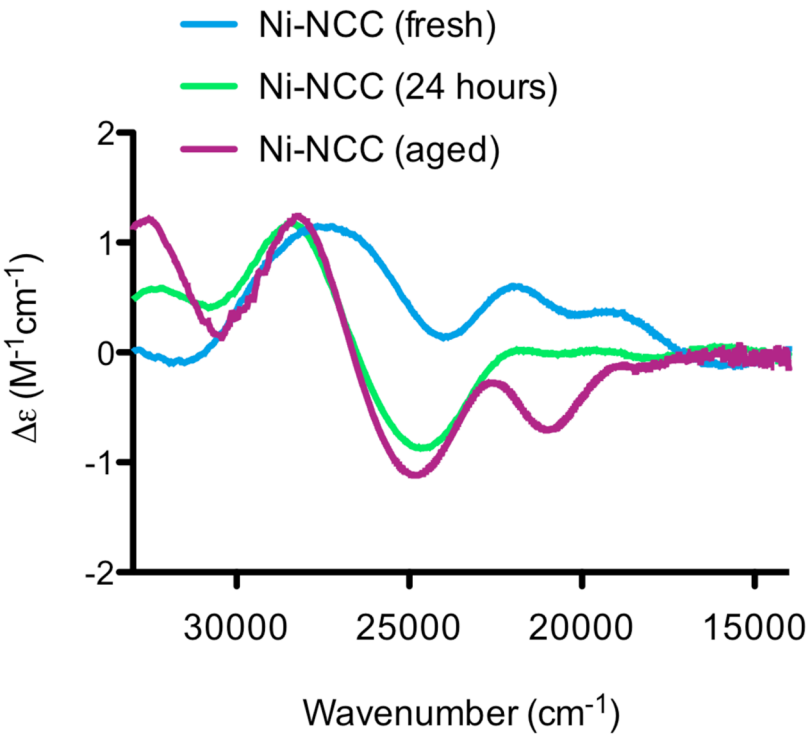

Figure 3.
Aging progression of Ni-NCC in phosphate. (Blue = fresh, Green = 24 hours, Pink = aged).

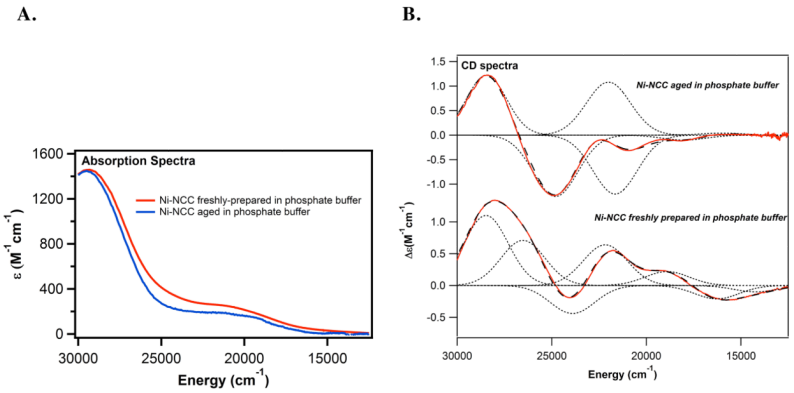

Figure 4.

(**a**) Electronic absorption spectra of freshly prepared (red) and aged (blue) Ni-NCC in 50 mM phosphate buffer at pH 7.4. (**b**) CD spectra of the same samples. Individual Gaussian curves (…) and their sums (- - -) obtained from fits of the CD data are displayed.

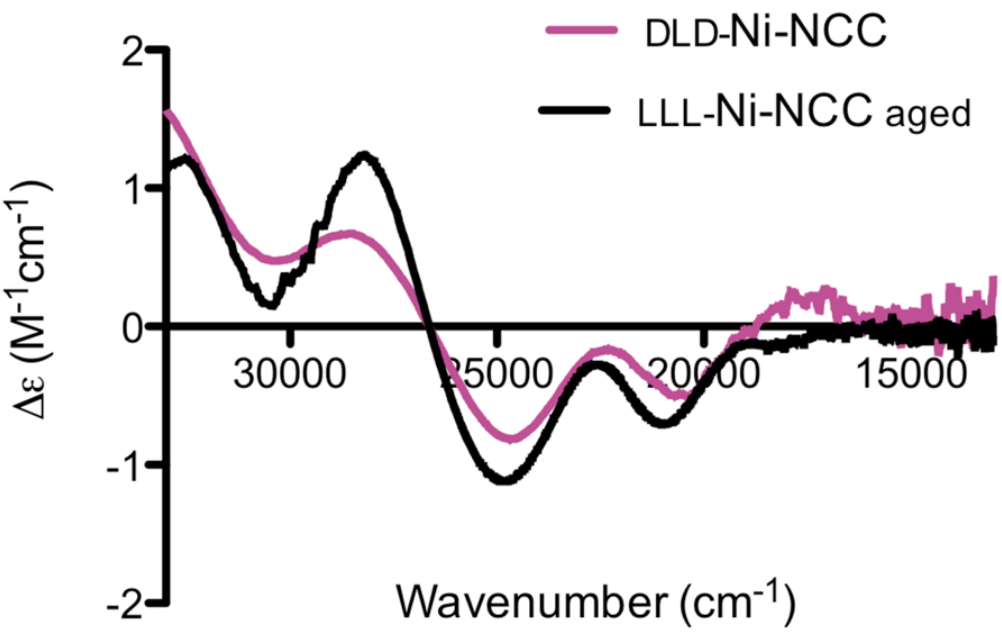

Figure 5.
CD spectra of Ni-NCC aged in phosphate buffer (black) vs. DLD-Ni-NCC (purple).

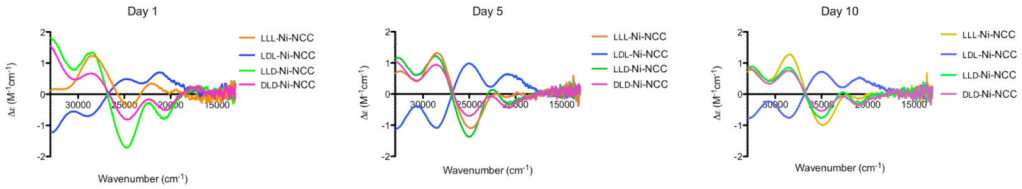

Figure 6.

CD spectra depict the aging progression of various chiral versions of the Ni-NCC complex. (Orange = NCC, Blue = LDL-Ni-NCC, Green = LLD-Ni-NCC, Pink = DLD-Ni-NCC.)

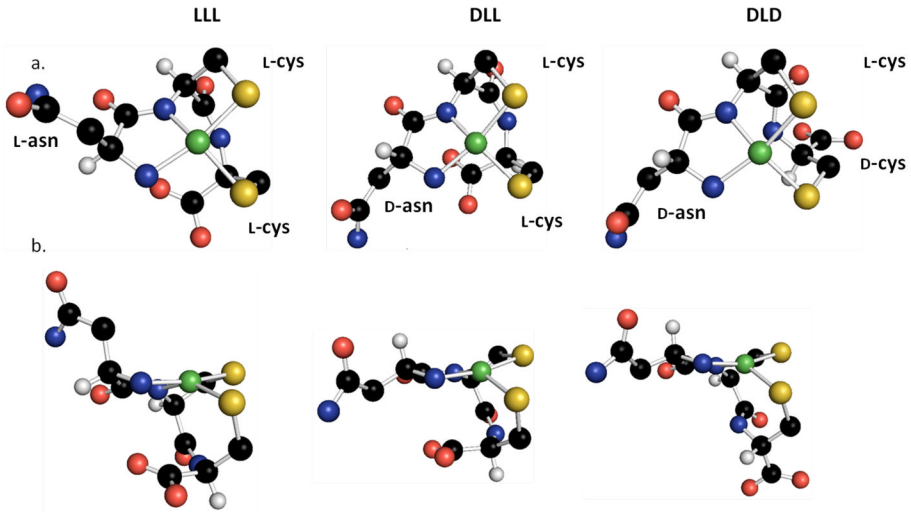

Figure 7.

Energy-minimized structures of LLL-, DLL-, and DLD-Ni-NCC. The only hydrogen atoms shown are those attached to the C_α of the residues. Views perpendicular to the square plane (a) and in the plane (b) are shown.

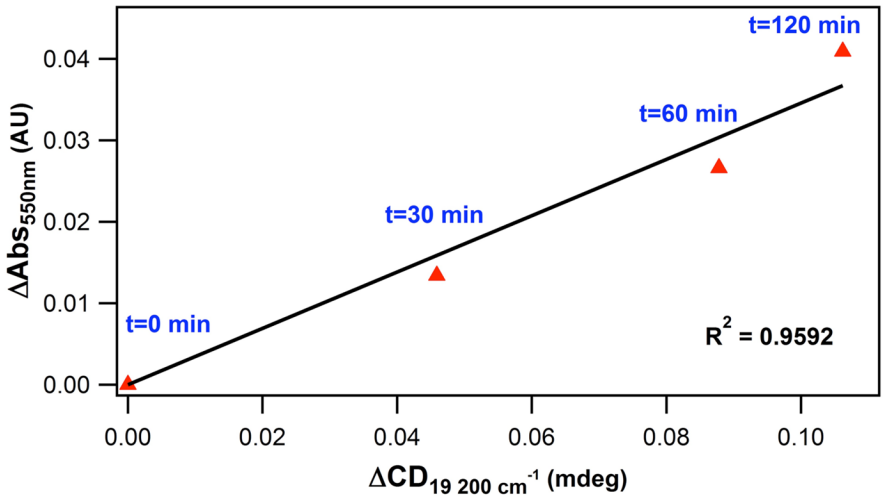

Figure 8.
Change in SOD activity of Ni-NCC as a function of structural change over time, as measured by CD spectroscopy.

Table 1

Transition energies derived from Gaussian deconvoluted CD spectra of freshly prepared and aged Ni-NCC in phosphate buffer. Bands having opposite sign in the fresh and aged spectra are shown in italics.

Band	Freshly Prepared		Aged	
	Δε ($M^{-1}cm^{-1}$)	Energy (cm^{-1})	Δε($M^{-1}cm^{-1}$)	Energy (cm^{-1})
1	−0.1	14200	*a*	*a*
2	*−0.21*	*16270*	*0.04*	*16000*
3	*0.22*	*18900*	*−0.1*	*18000*
4	*0.64*	*22170*	*−0.78*	*21600*
5	*−0.44*	*23900*	*0.7*	*22000*
6	*0.71*	*26520*	*−1.3*	*24800*
7	1.1	28475	1.22	28450

[a] The low signal-to-noise ratio between 11 000 and 14 000 cm^{-1} precludes reliable deconvolution within this spectral window.

Table 2

IR data for cyanide coordinated to nickel.

Species	ν(C≡N) (cm^{-1})
NaCN	2088
$K_2[Ni(CN)_4]$[42]	2123
Ni(CN)-(mSOD)[42]	2108
Ni-NCC + CN^- borate	2109
Ni-NCC + CN^- phosphate (fresh)	N/A
Ni-NCC + CN^- phosphate (aged)	2107

Table 3

Bond lengths (Å) and relative energies (kcal/mol) of DFT-optimized models of Ni^{II}-NCC with amino acids of differing chiralities.

	LLL-Ni-NCC	DLL-Ni-NCC	LDL-Ni-NCC	LLD-Ni-NCC	DDL-Ni-NCC	DLD-Ni-NCC
Ni-N_{amine}	1.976	1.972	1.974	1.982	1.979	1.990
Ni-N_{amide}	1.890	1.856	1.867	1.866	1.866	1.887
Ni-S_{cys2}	2.222	2.184	2.165	2.179	2.164	2.196
Ni-S_{cys3}	2.161	2.199	2.199	2.221	2.199	2.238
Relative Energy	0.0	−0.3	4.7	−11.6	5.1	−11.1

Table 4

TD-DFT computed *d-d* transition energies (cm^{-1}) for Ni-NCC models.

Band	LLL	DDL	DLD
1	14 500	15 500	12 400
2	15 600	16 600	14 300
3	17 000	17 300	15 600
4	19 300	18 800	18 500